EFDA–JET–PR(13)34

C. Bourdelle, C.F. Maggi, L. Chôné, P. Beyer, J. Citrin, N. Fedorczak,
X. Garbet, A. Loarte, F. Millitello, M. Romanelli, Y. Sarazin
and JET EFDA contributors

L to H Mode Transition: On the Role of Z_{eff}

L to H Mode Transition: On the Role of Z_{eff}

C. Bourdelle[1], C.F. Maggi[2], L. Chôné[3], P. Beyer[3], J. Citrin[1], N. Fedorczak[1],
X. Garbet[1], A. Loarte[4], F. Millitello[5], M. Romanelli[5], Y. Sarazin[1]
and JET EFDA contributors*

JET-EFDA, Culham Science Centre, OX14 3DB, Abingdon, UK

[1]*CEA, IRFM, F-13108 Saint-Paul-lez-Durance, France.*
[2]*Max Planck Institut fur Plasmaphysik, EURATOM Association, Garching, Germany*
[3]*PIIM - UMR 7345 - Université d'Aix-Marseille - CNRS, 13397 Marseille Cedex 20, France*
[4]*ITER Organization, Route de Vinon sur Verdon, 13115 St Paul Lez Durance, France*
[5]*EURATOM-CCFE Fusion Association, Culham Science Centre, OX14 3DB, Abingdon, OXON, UK*
** See annex of F. Romanelli et al, "Overview of JET Results",*
(24th IAEA Fusion Energy Conference, San Diego, USA (2012)).

Preprint of Paper to be submitted for publication in
Nuclear Fusion Letter

ABSTRACT

In this paper, the nature of the primary instability present in the pedestal forming region prior to the transition into H mode is analyzed using a gyrokinetic code on JET-ILW profiles. The linear analysis shows that the primary instability is of resistive nature, and can therefore be stabilized by increased temperature, hence power. Its growth rate reaches a minimum for a temperature corresponding to the magnitude of the experimentally measured temperature at the L-H transition. The minimum of the growth rate is shifted towards lower temperature for lower effective charge Z_{eff}. This dependence is shown to be in qualitative agreement with recent and past experimental observations of reduced Z_{eff} associated with lower L-H power thresholds.

INTRODUCTION

Recent observations of the impact of the ITER Like Wall (ILW) in JET show a L to H mode power threshold reduced by ≃ 40% in JET-ILW with respect to similar experiments in C wall [1, 2]. This reduction is observed on the high density branch. The experiments were carried out with slow power ramps and matched plasma shapes, divertor configurations and I_p = BT pairs. In ASDEX Upgrade, a similar reduction of the threshold when comparing C wall to metallic wall is observed [3] despite very different divertor configurations, geometries and wall materials. A common feature of both JET-ILW and ASDEX Upgrade is an observed significant reduction of the Z_{eff} when switching from C walls to metallic ones. In JET-ILW, the Z_{eff} reduction is more clearly observed at larger triangularities [2].

Numerous past results have shown that divertor geometry and plasma shape strongly impact the power threshold. The L-H threshold has been found to be lower by 20 to 35% with increased divertor closure in JET-C [4, 5] and in JT-60U [6]. Whereas, in ASDEX-Upgrade [7] and Alcator C-Mod [8] an increased divertor closure did not affect the L to H power threshold. In recent Alcator C-Mod experiments, the slot divertor configuration is associated with a lower power threshold than the vertical target configuration [9]. For both JET-C and JT60-U, during L mode phases, an increased divertor closure is associated with lower Z_{eff}. In Alcator C-Mod slot divertor, a lower radiated power from the bulk plasma [9] is reported. When reducing the neutrals in the main chamber, one also reduces the D_ρ emission. The link between a lower power threshold and a lower D_ρ emission is illustrated by the X-point height scan performed on DIII-D [10], where a lower X-point height leads to a lower threshold. A similar X-point height impact is also reported for JET-C [11]. A link between these various results can be that, through a modified divertor geometry and/or plasma shape, a reduced contamination of the plasma favors a lower L-H power threshold. Indeed, the plasma contamination can respond to reduced main chamber neutrals [4, 12], modified divertor screaning [13], divertor and wall temperatures [14], distance from the LCFS to the wall, SOL parallel flows, etc.

The link between a modified plasma shape and a modified Z_{eff} has been tested on recent JET-ILW data where five different configurations have been explored at 2.4T /2.0MA. Three configurations kept the upper triangularity (ρ_U) fixed to high values while moving the strike point positions; and two configurations kept the upper triangularity to a lower value while modifying the lower triangularity (ρ_L) [2]. A reduction of the power threshold (from 3MW down to 1.5MW) at constant density is observed to be correlated with a reduction of Z_{eff}, as illustrated by figure 1, rather than with modified ρ_U and ρ_L [2].

When changing from a C wall to a metallic wall or when modifying the divertor geometry and/or the plasma shape, the L to H power threshold is reduced as well as Z_{eff}, echoing the 2004 ITPA scaling [15] where a power threshold scaling with $\left(\frac{Z_{eff}}{2}\right)^{0.7}$ was proposed.

A power threshold lower with lower Z_{eff} suggests the existence of resistivity driven modes. Resistive modes named Resistive Ballooning Modes (RBM) have been proposed in the late '90s as plausible candidates to explain the L to H transition and the density limit [16]. Recently, in L mode edges RBM have been found linearly unstable [17].

In the following, JET-ILW data in L mode just prior to the L to H transition is analyzed. The code used is the linear version of the gyrokinetic turbulence code, GENE [18, 19]. The analyses are performed using fits of experimental data of the Pulse No: 82228 at $\rho = 0.97$, i.e. in the pedestal forming region. The electron temperature and density profiles are fitted and time averaged over 50ms. The electron temperature profile is based on High Resolution Thomson Scattering measurements as well as ECE. The electron density profile is using both HRTS and Li beam measurements. The alignment of the edge profiles with respect to the separatrix is improved by invoking the pressure balance along the magnetic field lines. However, a residual uncertainty of order 0.5cm still remains in the separatrix position. The relative position of the density and temperature are constrained thanks to a shared diagnostic, the HRTS. The ion temperature is taken to be equal to the electron temperature. This is justified by the edge charge exchange analysis carried out on some of the profiles at the L to H transition showing $T_i = T_e$ inside and up to the pedestal top [2]. The q profiles have been reconstructed using the HELENA equilibrium code [20], taking the pressure gradient from the fitted profiles. In this L mode phase, the bootstrap contribution is low and the q profiles are not very different from the ones provided by the standard EFIT analysis. Z_{eff} is provided by the horizontal line of sight of the Bremsstrahlung diagnostic. No local measurement of this quantity is available, therefore a flat Z_{eff} profile is assumed. The main parameters useful for the linear gyrokinetic analysis are summarized in the table below:

Before going further into the analysis, it is essential to note that the key ingredients to a microstability analysis are extremely demanding on the diagnostics precision. Indeed the local Z_{eff} is needed, as well as various gradient lengths. The q profile and its shearing are also essential. In this radial region where the toroidal rotation is low [2], the E×B shearing rate depends essential on the gradients of density and temperature gradients. These data are unfortunately subject to uncertainties. As a consequence, a gradient driven gyrokinetic analysis can mostly provide qualitative information. Quantitative information can be extracted only once the impact of the various uncertainties has been discussed.

Given the large uncertainties on the E×B shearing rate, and since the focus of this work is to investigate the nature of the primary instability, the E×B shearing rate is set to zero in GENE linear simulations.

GENE is using an adaptive time step scheme, which is a very useful feature to compute high collisionality cases. GENE is run linearly in its initial value version. The circular geometry is used. Typical GENE grid parameters are as follows: for the perpendicular grid discretization $n_x = 64$; in the parallel direction $n_z = 40$; 36 points are used in the parallel velocity direction; and 16 magnetic moments: the extension of the simulation box in the parallel velocity direction, in units of the thermal velocity, is 3; and the upper end of the simulation box in the magnetic moment direction, in units of T/B, is 9.

In this region, the gyro-ordering is respected. Indeed, the frequencies of the modes for $k_\rho\rho_s$ up to 0.4 are below $10^6 s^{-1}$ roughly two orders of magnitude below the ion cyclotron frequency at 1.8T: $8.6\times10^7 s^{-1}$. In the following, the analysis will focus on the modes stability at $k_\rho\rho_s = 0.1$, where the growth rates of the RBM are destabilized by higher collisionality, as already shown in [17]. Moreover, it is justified to focus the analysis on the low k_ρ modes since they are the ones contributing mostly to the transport. Concerning the local approximation, the radial extension over which the input parameters are roughly constant Δr is compared to the scale of the unstable modes ρ. The local approximation is valid if $\rho < \Delta r$. The temperature gradient length and the collisionality vary by ±30% over ρ = 0.94–0.99, hence over a radial extension $\Delta r \simeq 0.04$m. Now, one needs to compare Δr with a wavelength of the mode $\rho = \frac{2\rho}{k_\theta} = \frac{2\rho}{k_\theta\rho_s}\rho_S$, with $\rho_s = 8.9\times10^{-4}$m and $k_\rho\rho_s = 0.1$. Hence $\frac{\Delta\rho}{\rho} \simeq 0.8$ which is marginally satisfactory. The validity of the local approximation is therefore an open issue for this L mode edge region. The modes are analyzed at $k_\rho\rho_s = 0.1$. To represent a power ramp at a fixed density, the temperature is scanned. The normalized temperature gradient R/L_T is kept fixed, assuming stiff turbulence in L mode. Figure 2 illustrates a temperature scan with the other parameters fixed to the values given in table I for three values of Z_{eff}. As the temperature is increased, the modes are firstly stabilized. These modes are drifting in the electron direction and are stabilized by higher temperature, hence lower resistivity. They are identified as being Resistive Ballooning Modes [17]. As the temperature is further increased, the growth rates reach a minimum above which other modes drifting in the ion diamagnetic direction are destabilized. These modes correspond to the coupled Ion Temperature Gradient (ITG) and Trapped Electron Mode (TEM) system. These modes are more unstable as the collisionality is reduced [21]. As the temperature is increased, the collisionality decreases resulting in a competition between the stabilization of RBM and the destabilization of ITG-TEM. This leads to the existence of a temperature at which the growth rate is minimal. It is interesting to note that the temperature at which the growth rate is minimum, Tmin, is of the order of the experimental temperature prior to the tran sition. Indeed, for $Z_{eff} = 1.3$, T_{min} varies from 120 up to 160eV while varying the input parameters within reasonable uncertainties as summarized in table II. The experimental temperature value at ρ = 0.97 is 122eV as reported in Table I.

In predator-prey models describing the L to H mode transition, schematically, the transition occurs when the characteristic time of the predator becomes large enough compared to the characteristic time of the prey [22–24]. A similar ratio of characteristic times is used to model Internal Transport

Barriers [25]. In [26], such an empirical time ratio allows to constrain the L to H power threshold. Recently, numerous experimental results on the dynamics of the L to H transition have been compared to predator-prey models [27–29]. Nonetheless, the nature of the predator (zonal and/or mean flows) remains an open issue for the time being. Concerning the nature of the prey, for core ITB models, the prey is an ITG type of mode [25]. At the edge, the nature of the mode is not precisely defined. On the experimental side, the nature of the turbulence at the edge in L mode has yet to be identified and its nature presently challenges non-linear gyrokinetic numerical simulations [30]. The work presented here suggests that RBM could be identified to the prey. In such a framework, the transition into H mode, linked to the ratio of the characteristic time of the predator to characteristic time of the prey (1/ρ where ρ is the growth rate), is likely to be facilitated as the primary instability is weakened. Therefore, in the following, we will address the impact of Z_{eff} and density on the primary instability of the JET-ILW case analyzed.

For the 1.8T = 1.7MA cases, Z_{eff} of JET-ILW ranges from 1.2 to 1.4 depending on the density, whereas the values of Zeff in the JET-C cases vary from 1.5 to 2.4 depending on the density and on the triangularity [2]. The variation of Z_{eff} is clearer in the high triangularity 3T = 2:75MA data where Z_{eff} in JET-C stands around 1.9-2.3, and in JET-ILW around 1.1-1.4 [2]. Therefore, to qualitatively imitate the impact of the wall modification on Zeff , Zeff is chosen to increase from 1:3 with a mix of D and Be up to 2:2 with a mix of D and C. Now, to mimic the plasma shape impact illustrated by figure 1, Zeff is increased from 1 up to 1:3, with a mix of D and Be. By increasing Zeff at a given temperature, the resistivity is increased and leads to more unstable RBM. On the contrary, high Zeff provokes dilution and stabilizes both ITG and TEM [31]. Therefore, increasing Zeff reduces the growth rates at low temperature and shifts Tmin to higher values as illustrated in figure 2. This shift of Tmin is in qualitative agreement with the shift of the L to H threshold towards higher power at higher Zeff .

The density has a strong impact on the L to H power threshold. At low densities, a low density branch is reported in JET-ILW [1, 2] in which the L-H transition power increases with decreasing density. On the other hand, the higher density branch, where the power threshold increases with higher density [32], is always observed in all kind of machines and configurations. To study the impact of a modified density on the temperature scan where the RBM and the ITG-TEM are competing, one can repeat the same temperature scan for lower densities. The reference density used so far, $2.6\times10^{19}m^{-3}$, is compared to $1\times10^{19}m^{-3}$3 and $0.4\times10^{19}m^{-3}$. If the density is increased, the collisionality increases leading to stronger RBM and weaker ITG-TEM, resulting in a robust shift of Tmin towards higher values. This behavior is in qualitative agreement with a higher power threshold at higher density. This is what is reported in figure 3. Figure 3 could be compatible with the existence of a minimum in density for temperatures ranging from 100eV to 150eV, where the growth rates at $1\times10^{19}m^{-3}$ are lower than the growth rates at both lower and higher densities. But this qualitative explanation requires that, for some unknown reason, the lowest density case enters into H mode at a temperature larger than Tmin.

Based on the recent JET-ILW power threshold experiments analysis [2], Z_{eff} is shown to a be a potential candidate explaining a lower power threshold in JET-ILW when compared to similar JET-C pulses. It is also shown that, by changing the divertor configuration by varying the lower and upper triangularities in JET-ILW, the power threshold decreases linearly as Z_{eff} is decreased. Former results on the X point height and divertor closure impact on the power threshold are reviewed and also point towards the potential role of a modified Zeff impacting the threshold as previously proposed for the ITPA- 2004 power threshold scaling law [15].

A linear gyrokinetic stability analysis is performed with GENE [18]. The input data are based on JET-ILW profiles prior to the L to H mode transitions. To represent a power ramp at fixed density, the temperature is scanned in GENE. At low temperature, Resistive Ballooning Modes are unstable. As the temperature is increased, the resistivity is reduced, and the modes are stabilized. When increasing further the temperature, ITG-TEM take over and are further destabilized as the collisionality is reduced. The competition between stabilized RBM and destabilized ITG-TEM lead to a growth rate which is minimum at a given temperature. Assuming that the L to H mode transition is explained by a predator-prey mechanism, the entry into H mode is facilitated when the characteristic time of the predator is enhanced or when the characteristic time of the prey (/ 1=) is weakened. The RBM are proposed as being the prey. Therefore the transition into H mode is expected to be facilitated when the RBM growth rates are reduced, hence at a temperature around the minimal growth rate. Within the uncertainties on various input parameters (R/L_T,s, etc), the temperature at which the growth rates reach a minimum (120–160eV) is in agreement with the experimentally measured value, 122eV. For a larger Z_{eff} , the temperature of the minimum growth rate is shifted towards larger values. This observation is in qualitative agreement with the need for a larger power to access H mode in JET-C wall compared to the JET-ILW and with the correlation of the power threshold with Z_{eff} when changing the divertor configurations. For larger density, the temperature of the minimum growth rate is also shifted towards larger values, in qualitative agreement with the L-H power threshold scaling laws such as [32].

To go further than the present first insights into the L to H mode transition, both the prey and the predator mechanisms need to be self-consistently modeled. The E×B shearing rate impact on the linear mode has to be investigated. It should be done on experiments where the uncertainties on E_r are minimized [33]. Non-linearly, flux driven codes are able to shed light on the predator-prey interplay. An effort using the electromagnetic fluid code EMEDGE3D is presently ongoing including both the self-consistent mean and zonal flows evolution as well as non-linear RBM, the first promising results are presented in [34].

ACKNOWLEDGMENTS
The GENE development team efficiency in guiding GENE users and in sorting out numerical issues is deeply thanked. Ph. Ghendrih and R. Sabot are thanked for their active participation to fruitful working discussions at IRFM. Y. Camenen, G. Fuhr, A. Monnier are thanked for useful, stimulating discussions at the Université d'Aix-Marseille. S. Saarelma is thanked for providing an appreciated help to compute the selfconsistent HELENA equilibrium.

This research used resources of the National Energy Research Scientific Computing Center, which is supported by the Office of Science of the U.S. Department of Energy under Contract No. DE-AC02-05CH11231.

This work, supported by the European Communities under the contract of Association between EURATOM and CEA, was carried out within the framework of the European Fusion Development Agreement. The views and opinions expressed herein do not necessarily reflect those of the European Commission or the ITER Organization.

REFERENCES

[1]. Maggi C.F. et al. 39th EPS Conference on Controlled Fusion and Plasma Physics, Stockholm, 2012.

[2]. Maggi C.F. et al. submitted to Nuclear Fusion, 2013.

[3]. R. Neu et al. Journal of Nuclear Materials, 438, Supplement (0):S34 – S41, 2013.

[4]. L.D Horton, G.C. Vlases, P. Andrew, V.P Bhatnagar, A.V. Chankin, S Clement, GD Conway, SJ Davies, J.C.M de Haas, JK Ehrenberg, G.M Fishpool, E Gauthier, H.Y Guo, P.J Harbour, L.C. Ingesson, H.J Jackel, J. Lingertat, A. Loarte, C.G. Lowry, C.F. Maggi, G.F. Matthews, G.M. McCracken, R. Mohanti, R.D. Monk, R. Reichle, E. Righi, G. Saibene, R. Sartori, R. Simonini, M.F. Stamp, A. Taroni, and K. Thomsen. Studies in JET diverters of varied geometry. I: Non-seeded plasma operation. Nuclear Fusion, **39**(1):1–17, JAN 1999.

[5]. Y Andrew et al. Plasma Physics and Controlled Fusion, 46(5A):A87, 2004.

[6]. T Fukuda, T Takizuka, K Tsuchiya, Y Kamada, and N Asakura. Reduction of L-H transition threshold power under the Wshaped pumped divertor geometry in JT-60U. Plasma Physics and Controlled Fusion, **42**(5A):A289–A297, May 2000. 7th IAEA Technical Committee Meeting on H-Mode and Transport Barrier Physics, Oxfoed, England, September 27-29, 1999.

[7]. Bosch HS. Journal of Nuclear Materials, **266**:462, 1999.

[8]. Pitcher C.S. Physics of Plasmas, **7**:1894, 2000.

[9]. Y. Ma, J.W. Hughes, A.E. Hubbard, B. LaBombard, R.M. Churchill, T. Golfinopolous, N. Tsujii, and E.S. Marmar. Scaling of h-mode threshold power and lâ˘A ¸Sh edge conditions with favourable ion grad- b drift in alcator c-mod tokamak. Nuclear Fusion, **52**(2):023010, 2012.

[10]. P. Gohil, T.E. Evans, M.E. Fenstermacher, J.R. Ferron, T.H. Osborne, J.M. Park, O. Schmitz, J.T. Scoville, and E.A. Unterberg. Nuclear Fusion, **51**(10):103020, 2011.

[11]. Y. Andrew, T.M. Biewer, K. Crombe, D. Keeling, E. de la Luna, C Giroud, N.C. Hawkes, M Kempenaars, A. Korotkov, A. Meigs, Y.R. Martin, A Murari, I Nunes, R. Sartori, T. Tala, and JET EFDA contributors. H-mode access on jet and implications for iter. Plasma Physics and Controlled Fusion, **50** (12):124053, 2008.

[12]. A. Loarte. Effects of divertor geometry on tokamak plasmas. Plasma Physics and Controlled Fusion, **43** (6):R183–R224, JUN 2001.

[13]. H.Y. Guo, G.F. Matthews, I. Coffey, S.K. Erents, M. Groth, P.J. Harbour, M.G. von Hellermann,

D.L. Hillis, J.T. Hogan, L.D. Horton, L.C. Ingesson, K.D. Lawson, J. Lingertat, C.F. Maggi, G.M. Mc- Cracken, R.D. Monk, P.D. Morgan, M.F. Stamp, P.C. Stangeby, A. Taroni, and G.C. Vlases. Effects of divertor geometry and chemical sputtering on impurity behaviour and plasma performance in JET. Nuclear Fusion, **40** (3):379–396, MAR 2000.

[14]. GM McCracken, R Barnsley, HY Guo, MG von Hellermann, LD Horton, HJ Jackel, J Lingertat, CF Maggi, GF Matthews, RD Monk, MG O'Mullane, MF Stamp, PC Stangeby, GC Vlases, and KD Zastrow. Studies in JET diverters of varied geometry. III: Intrinsic impurity behaviour. Nuclear Fusion, **39** (1):41–60, JAN 1999.

[15]. T. Takizuka and ITPA H-Mode Database Working Grp. Roles of aspect ratio, absolute B and effective Z of the H-mode power threshold in tokamaks of the ITPA database. Plasma Physics and Controlled Fusion, **46** (5A):A227–A233, May 2004. 9th IAEA Technical Meeting on H-mode Physics and Transport Barriers, San Diego, CA, SEP 24-26, 2003.

[16]. B.N. Rogers, J.F. Drake, and A. Zeiler. Phase space of tokamak edge turbulence, the L–H transition, and the formation of the edge pedestal. Physical Review Letters, **81** (20):4396–4399, 1998.

[17]. C. Bourdelle, X. Garbet, R. Singh, and L. Schmitz. Plasma Physics and Controlled Fusion, **54** (11):115003, 2012.

[18]. F. Jenko. Computer Physics Communications, **125**(1-3):196–209, 2000.

[19]. S. Brunner T. Dannert F. Jenko F. Merz T. Gãürler, X. Lapillonne and D. Told. Journal of Computational Physics, **230**:7053, 2011.

[20]. Huysmans G.T.A., Goedbloed J.P., and Kerner W. CP90 Conf. on Comp. Physics, page 371, 1991.

[21]. M. Romanelli, G. T. Hoang, C. Bourdelle, C. Gormezano, E. Giovannozzi, M. Leigheb, M. Marinucci, D. Marocco, C. Mazzotta, L. Panaccione, V. Pericoli, G. Regnoli, O. Tudisco, and F. T. U. Team. Parametric dependence of turbulent particle transport in high density electron heated ftu plasmas. Plasma Physics and Controlled Fusion, **49** (6):935–946, 2007.

[22]. Sanae-I. Itoh, Kimitaka Itoh, Atsushi Fukuyama, and Yukitoshi Miura. Edge localized mode activity as a limit cycle in tokamak plasmas. Physical Review Letters, **67**:2485–2488, Oct 1991.

[23]. Eun-jin Kim and P.H. Diamond. Zonal flows and transient dynamics of the L–H transition. Physical Review Letters, **90**:185006, May 2003.

[24]. K. Miki, P. H. Diamond, Oe. D. Guercan, G.R. Tynan, T. Estrada, L. Schmitz, and G.S. Xu. Spatio-temporal evolution of the L -> I -> H transition. Physics of Plasmas, **19**(9), SEP 2012.

[25]. R.E. Waltz, G.M. Staebler, W. Dorland, G.W. Hammett, M. Kotschenreuther, and J.A. Konings. A gyro-Landau-fluid transport model. Physics of Plasmas, **4**(7):2482–2496, JUL 1997.

[26]. W. Fundamenski, F. Militello, D. Moulton, and D.C. McDonald. A new model of the L–H transition in tokamaks. Nuclear Fusion, **52**(6):062003, 2012.

[27]. L. Schmitz, L. Zeng, T. L. Rhodes, J. C. Hillesheim, E. J. Doyle, R. J. Groebner, W. A. Peebles,

K.H. Burrell, and G. Wang. Role of zonal flow predator-prey oscillations in triggering the transition to h-mode confinement. Physical Review Letters, **108**:155002, Apr 2012.

[28]. G.R. Tynan, M. Xu, P.H. Diamond, J.A. Boedo, I. Cziegler, N. Fedorczak, P. Manz, K. Miki, S. Thakur, L. Schmitz, L. Zeng, E.J. Doyle, G.M. McKee, Z. Yan, G.S. Xu, B.N. Wan, H.Q. Wang, H.Y. Guo, J. Dong, K. Zhao, J. Cheng, W.Y. Hong, and L.W. Yan. Turbulent-driven low-frequency sheared e Ã°U b flows as the trigger for the h-mode transition. Nuclear Fusion, **53**(7):073053, 2013.

[29]. T. Kobayashi, K. Itoh, T. Ido, K. Kamiya, S.-I. Itoh, Y. Miura, Y. Nagashima, A. Fujisawa, S. Inagaki, K. Ida, and K. Hoshino. Spatiotemporal structures of edge limit-cycle oscillation before l-to-h transition in the jft-2m tokamak. Nuclear Fusion, **111**:035002, Jul 2013.

[30]. C. Holland, L. Schmitz, T. L. Rhodes, W.A. Peebles, J.C. Hillesheim, G. Wang, L. Zeng, E.J. Doyle, S.P. Smith, R. Prater, K.H. Burrell, J. Candy, R.E. Waltz, J.E. Kinsey, G.M. Staebler, J.C. DeBoo, C.C. Petty, G.R. McKee, Z. Yan, and A.E. White. Advances in validating gyrokinetic turbulence models against l- and h-mode plasmas. Physics of Plasmas, **18**(5), 2011.

[31]. C. Bourdelle, X. Garbet, G.T. Hoang, J. Ongena, and R.V. Budny. Nuclear Fusion, **42** (7):892, 2002.

[32]. Y.R. Martin, T. Takizuka, and the ITPA CDBM H-mode Threshold Database Working Group. Journal of Physics: Conference Series, 123(1):012033, 2008.

[33]. E. Viezzer, T. PÃijtterich, G.D. Conway, R. Dux, T. Happel, J.C. Fuchs, R.M. McDermott, F. Ryter, B. Sieglin, W. Suttrop, M.Willensdorfer, E.Wolfrum, and the ASDEX Upgrade Team. High-accuracy characterization of the edge radial electric field at asdex upgrade. Nuclear Fusion, **53** (5):053005, 2013.

[34]. L. Chôné, P. Beyer, Y. Sarazin, G. Fuhr, C. Bourdelle, and S. Benkadda. 40th EPS Conference on Controlled Fusion and Plasma Physics, Helsinki, 2013.

Pulse No:	ρ	R/L_T	R/L_n	T	n	ν^*	q	s	Z_{eff}	B
82228	0.97	55	9	122	2.6	9.2	3.8	4.3	1.3	1.8

Table I: Edge parameters for a JET-ILW Pulse No: 82228 prior to the L to H transition. The temperature is given in eV , the density n in $10^{19}m^{-3}$ and the magnetic field B in T.

Input parameters	ref case, table I	R/L_T = 30 (55)	R/L_n = 4 (9)	s = 2 (4.3)	q = 3 (3.8)
Temperature of min(γ) (eV)	$\simeq$ 160	$\simeq$120	$\simeq$160	$\simeq$160	$\simeq$ 120

Table II: The temperature of the minimum growth rate tested versus various input parameter uncertainties.

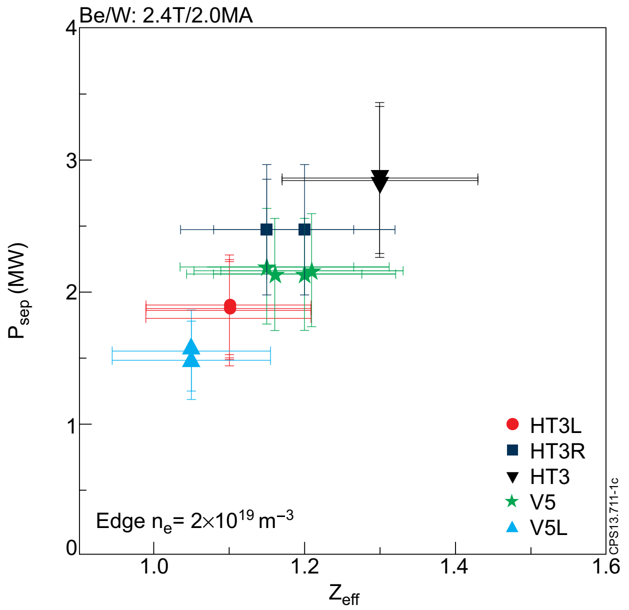

Figure 1: Variation of P_{sep} with Z_{eff} with JET-ILW at 2.4T/2.0MA (ICRH heating only) and constant plasma density, $n_e \cong 2\times10^{19} m^{-3}$, corresponding to nmin at this I_p/B_T. The acronyms in the legend correspond to the five magnetic configurations illustrated in greater details in [2]. HT3L: $\rho_U = 0.37$, $\rho_L = 0.41$; HT3R: $\rho_U = 0.38$, $\rho_L = 0.35$; HT3: $\rho_U = 0.395$, $\rho_L = 0.33$; V5L: $\rho_U = 0.19$, $\rho_L = 0.395$; V5: $\rho_U = 0.195$, $\rho_L = 0.33$.

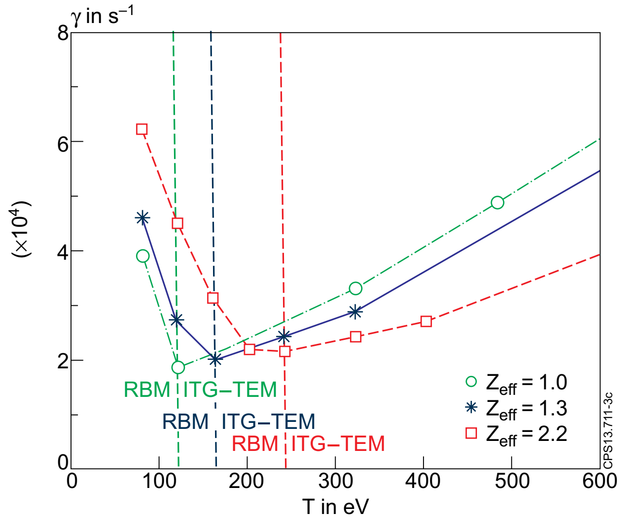

Figure 2: Growth rate of the most unstable mode at $k_\theta\rho_s$ = 0:1 versus the temperature for the parameters as given in table I, i.e. Z_{eff} = 1.3, blue asterisks. Green squares: same as asterisks but with Z_{eff} = 1. Red circles: same as asterisks but with Z_{eff} = 2.2.

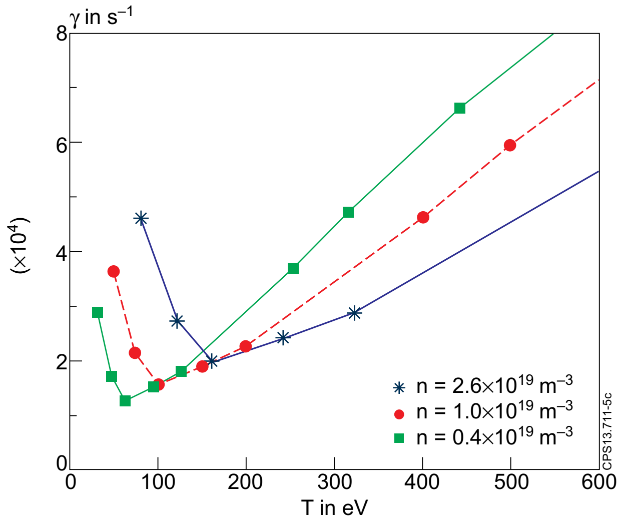

Figure 3: Growth rate of the most unstable mode versus the temperature for the parameters as given in table I, except changing n from 2.6×10^{19} m^{-3} down to 1×10^{19} m^{-3} and 0.4×10^{19} m^{-3}.